CHAPTER

9

Indo-Ganges River Basin Land Use/ Land Cover (LULC) and Irrigated Area Mapping

*Murali Krishna Gumma**, *Prasad S. Thenkabail*†, *Pardhasaradhi Teluguntla*†, *Anthony M. Whitbread**

*International Crops Research Institute for the Semi-Arid Tropics (ICRISAT), Patancheru, India
†U.S. Geological Survey (USGS), Western Geographic Science Center, Flagstaff, AZ, USA

9.1 INTRODUCTION

Geo-spatial information on the distribution of irrigated areas is limited to district-level crop statistics published by state or national governments in different parts of the world. Although data that has been collected by irrigation and agriculture departments are available, there are often differences between sources in regard to the extent of the irrigated areas (Biggs et al., 2006; Gumma, 2008). The World Summit on Sustainable Development (WSSD) organized by the United Nations and held at Johannesburg, South Africa, declared water as the most critical resource in the 21st century, with increasing demands and decreasing supplies. Much of the freshwater is consumed by irrigation and evapotranspiration from different land use/land cover (LULC) classes, especially through transpiration from natural vegetation. Of the different types of LULC classes, irrigation is known to consume about 60% of the world's available freshwater resources. With ballooning global populations projected to be 8.3 billion in 2030 compared to just over 6 billion at present and with food and nutritional intake expected to increase from 2500 cal to 3000 cal per day per person (FAO, 2003), the demand for water for irrigation will only grow. This is neither feasible due to a shortage of resources nor desirable due to the, still to be fully understood, environmental impacts of large, medium, and even small irrigation schemes on natural environments along river courses.

https://doi.org/10.1016/B978-0-12-812782-7.00010-2

Given the importance of irrigation to the world's food bank, a calculation of water resources that includes a detailed, accurate, and sophisticated LULC system is required. Land cover is likely to be the single most important factor of change in all river basins. It is well established that LULC changes have a significant effect on many processes in basins, including soil erosion, global warming (Penner et al., 1994), and biodiversity impacts (Chapin et al., 2000), and such changes are expected to have a greater influence on human habitability than climate change will (Skole, 2004). Through the use of the AVHRR pathfinder data sets, several global LULC maps have been produced (e.g., De Fries et al., 1998; Loveland et al., 2000).

Accurate information on the extent of river basin cropland is critical for food security assessments, water allocation decisions, and yield estimations. This information will also help decision makers monitor dynamic landscapes, such as agricultural lands, fallow croplands, and land cover such as forests, water bodies, and wetlands. Ex-ante assessments on the effect of changes in land use will facilitate sustainable land use planning, socially, economically, and ecologically. Moreover, countries' departments of agriculture and revenue will need such spatial information at the village-level in order to send advisories to farmers on timely inputs and best practices for agricultural management.

Croplands in the Indo-Ganges River Basin are frequently affected by abiotic stresses such as drought. Crop year 2015 was declared the hottest year on record by the world Meteorological Organization (WMO). Very high temperatures over both land and ocean in 2015 were accompanied by many extreme weather events, such as heatwaves, flooding, and severe drought (WMO, 2015). Several studies have been conducted on land use mapping and changes. However, the main purpose for analyzing changes in agricultural land use is to monitor cropping patterns and cropland changes (Singh, 1989; Wan et al., 2004; Yaduvanshi et al., 2015; Hao et al., 2016; Li et al., 2016; Olsson et al., 2016; Wang et al., 2016). These analyses rely heavily on agricultural statistics (e.g., extent of area). Besides discrepancies at the district, state, and provincial levels, there are discrepancies in the statistics reported by agricultural agencies and irrigation agencies. Variations in land use on such a large scale are not sufficient to fully clarify their effect on river basins. On the other hand, remote sensing with satellite imagery can give detailed maps of land use and identify where significant cropping pattern changes have occurred in response to variations in rainfall (Badhwar, 1984; Thiruvengadachari and Sakthivadivel, 1997). Remote sensing utilizing satellite imagery has been used to quantify water use and productivity in irrigation systems (Thiruvengadachari and Sakthivadivel, 1997), but is less frequently used to identify changes in irrigated command areas in response to variations in rainfall and water supply. Normalized Difference Vegetation Index (NDVI) time-series data have been used for mapping land use changes (Gumma et al., 2011b) and irrigated areas (Biggs et al., 2006; Thenkabail et al., 2009b). Time series data have also been used for detecting changes in irrigated areas in major river basins (Bhutta and Van der Velde, 1992; Gaur et al., 2008).

The present study analyzed the spatial extent of major croplands along with other LULC in the Indo-Ganges Basin. Water deficiency for rainfed crops was assessed based on low rainfall, which was reflected in the NDVI imagery from the 2013–14 period. The area under each type of land use for each year and the changes between years were estimated.

The estimates of both land use and land cover changes were compared with ground survey data and secondary sources, such as published statistics on rice systems. The focus was on the areas where significant changes had occurred in the cropping pattern.

In addition to the preceding assessments, the overarching goal of this study was to map the spatial extent of the above-mentioned croplands. The study used MODIS 250 m time-series data to map major croplands using SMTs that were first advocated for cropland mapping by Thenkabail et al. (2007) and later successfully applied in global and regional mapping of croplands (Thenkabail et al., 2007a, 2009a, 2012; Biradar et al., 2009; Pittman et al., 2010; Gray et al., 2014; Gumma et al., 2015a; Salmon et al., 2015; See et al., 2015).

9.2 STUDY AREA

The study area (see nonhatched area in the basin boundary in Fig. 9.1) covers 63% (133,071,400 ha) of the Indo-Gangetic Plain (total area = 217,699,000 ha.). Crop year 2013 was a normal year and 204 areas had significant rainfall deficit in terms of amount and

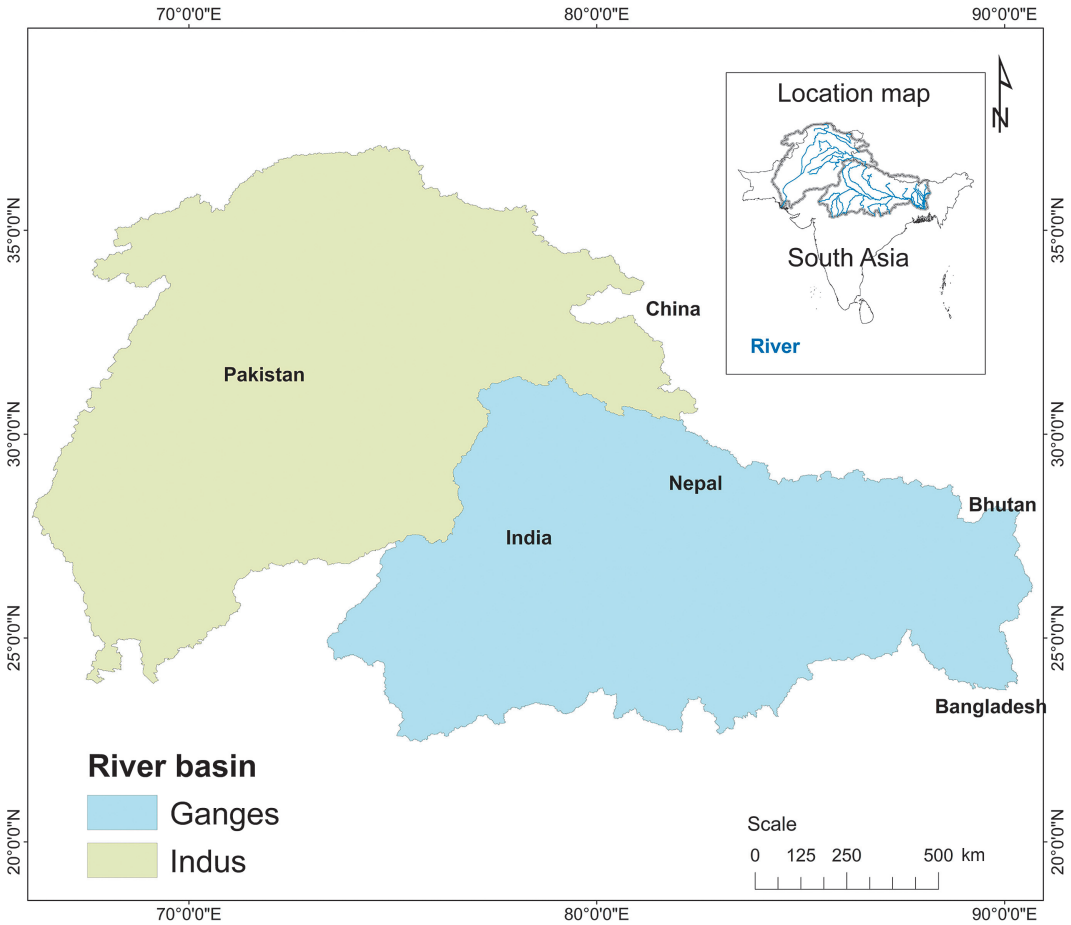

FIG. 9.1 Study area of Indo-Ganges River Basin.

distribution (Fig. 9.2). The area of the Ganges and the Indus basins falling within the three MODIS tiles (h24v06, h25v06, and h26v06; each tile is 1000 by 1000 km) was chosen as the area of study. The three tiles were mosaic tiles stacked into a single contiguous tile by running batch scripts in ERDAS Imagine 8.6 (ERDAS, 2003) from which the areas in the Ganges and Indus basins were delineated (Fig. 9.1). About 95% of the Ganges Basin (total area 95,111,154 ha.) and 37% of the Indus Basin (116,113,290 ha.) were covered by the three MODIS tiles. The characteristics of the 7-band, 8-day interval MODIS data of years 2001 and 2002 used in this study are shown in Fig. 9.1 and Table 9.1.

The origin of the Ganges River Basin is a highly fertile glacier called Gangotri, which is located in the Himalayans about 4267 m above sea level. The Ganges River Basin encompasses an area with a very high population density of about 530 persons per square kilometers, with the river flowing through 29 cities with populations of more than 100,000, 23 cities with populations between 50,000 and 100,000, and about 48 towns (Aitken, 1992; Ilich, 1996).

The source of the Indus River lies in Western Tibet in the Mount Kailas region at an altitude of 5500 m a.s.l. The Indus Basin comprises the Indus River, its five major left bank tributaries, the Jhelum, Chenab, Ravi, Beas, and Sutlej Rivers, and one major right bank tributary, the Kabul (Khan, 1999). The catchments contain some of the largest glaciers in the world

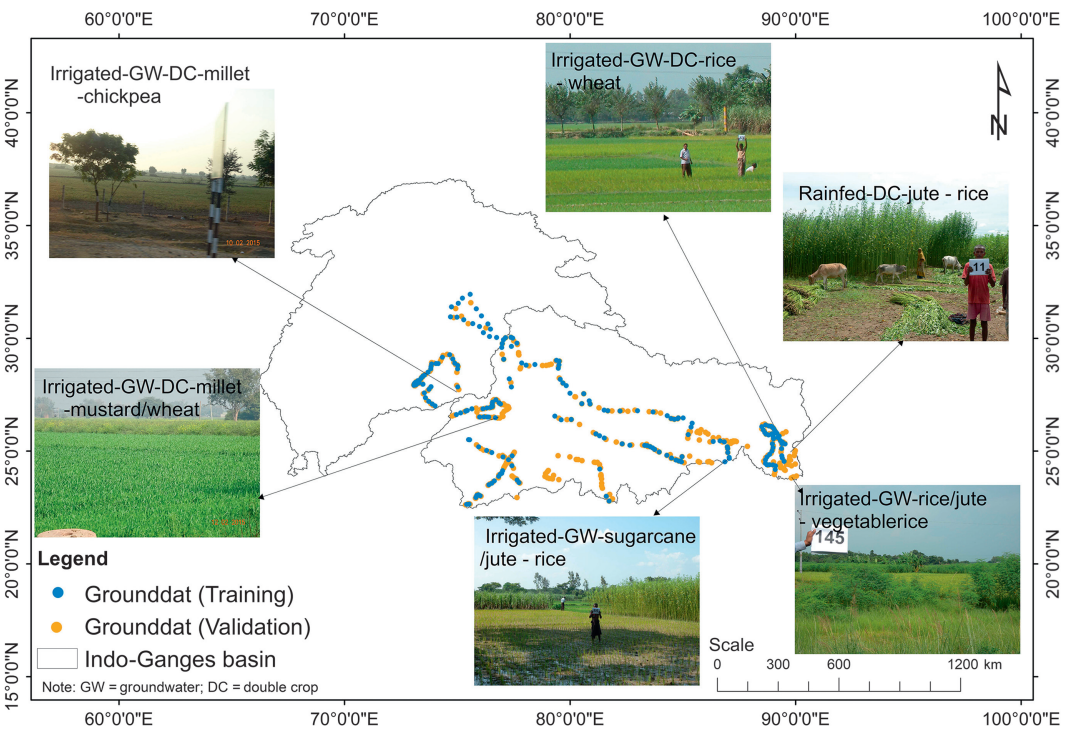

FIG. 9.2 Spatial distribution of ground data in Indo-Ganges River Basin.

TABLE 9.1 Total Geographical Area

Country	Total Geographical Area ('000 ha)	Area Covered in Indo-Ganges Region ('000 ha)	Percent of Indo-Ganges Basin (%)
Bangladesh	14,804	4273	2.0
Bhutan	4365	1816	0.8
India	345,623	123,795	56.9
Nepal	16,210	14,762	6.8
Pakistan	89,167	53,916	24.8
Afghanistan	65,200	7270	3.3
China	9,596,960	11,868	5.5
Total	1,01,32,329	217,699	

outside the polar regions (Meadows, 1999). Only 37% of the total basin area is covered in this study (Fig. 9.1), but much of this area covers the Punjab and Sindh regions, which are heavily irrigated by the Indus River.

9.3 DATA

9.3.1 Satellite Data

The MODIS data we used for the Krishna River Basin is archived at the NASA-USGS website (http://e4ftl01.cr.usgs.gov/MOLT/MOD13Q1.005). MODIS 2013–2014, recorded every 16 days (Table 9.2), and Terra sensor data were used for the present study. The format has two specific bands (band 1, red; and band 2, near infrared) that are processed for land applications as a MODIS vegetation index product (MOD13Q1). MOD13Q1 is computed from MODIS level 5 bands 1–2 (centered at 648 nm and 858 nm).

MODIS imagery was used to map the spatial extent of land use/land cover for the years 2013–14 and 2015–16. The process began with rescaling 16-day NDVI images that were later stacked into a single file data composite for each cropping year (Thenkabail et al., 2005; Dheeravath et al., 2010; Gumma et al., 2011a, 2015b). MODIS 16-day composites were converted into a NDVI monthly Maximum Value Composite (MVC) (NDVI MVC) using Eq. (9.1) (Casanova et al., 1998), where MVCi is the monthly MVC of the ith month and $i1$ and $i2$ represent all the 16-day data in a month:

$$\mathrm{NDVI}_{\mathrm{MVC}_i} = \mathrm{Max}\,(\mathrm{NDVI}_{i1,}, \mathrm{NDVI}_{i2,}) \tag{9.1}$$

In the present study, monthly NDVI MVC images were used for classification and a NDVI 16-day data set was used for identifying and labeling land use/land cover classes, including irrigated areas. The main reason for using MVC was to avoid noise (clouds) in some of the areas (Gumma et al., 2014).

TABLE 9.2 MODIS—250 m Terra Vegetation Indexes 16-Day L5 Product Used in This Study

MODIS Data Sets	Units	Band Width nm/Range	Potential Application
250 m 16 days NDVI	NDVI	−1 to +1	Vegetation conditions
250 m 16 days EVI	EVI	−1 to +1	Canopy structural variations
250 m 16 days red reflectance (Band 1)	Reflectance	620–670	Absolute land cover transformation, vegetation chlorophyll
250 m 16 days NIR reflectance (Band 2)	Reflectance	841–876	Cloud amount, vegetation land cover transformation
250 m 16 days blue reflectance (Band 3)	Reflectance	459–479	Soil/vegetation differences
250 m 16 days MIR reflectance (Band 7)	Reflectance	2105–2155	Cloud properties, land properties

9.3.2 Ground Data

Ground data was collected in 2013 from September 13 to September 26 for 227 sample points and in 2015 from September 21 through September 30 for 326 sample points covering about 8000 km of road travel in the Indo-Ganges Basin (Fig. 9.2). Ground data were collected based on pre-classified output, Google Earth imagery, and tracking GPS attached to the image processing software that captured ground survey information while in motion. Detailed information was collected for class identification and for labeling point locations. Point-specific information was collected from 250 m × 250 m plots and consisted of GPS locations, land use categories, land cover percentages, cropping patterns during different seasons (through farmer interviews), crop types, and watering methods (irrigated, rainfed). Samples were obtained within large contiguous areas of a particular LULC. Landsat 8 products were used as additional ground survey information in class identification. A stratified systematic sample design was adopted based on road network or footpath access. Where possible, a systematic location of sites was done every 5 km or 10 km along the road network by vehicle or by foot (Thenkabail et al., 2004, 2005; Gumma et al., 2011e), which is detailed in a description of the ground survey methodological approach.

9.3.3 Ideal Spectra Signatures

Ideal spectra signatures (Fig. 9.3) were generated using 16-day NDVI time-series composite and precise ground survey information that was also used for the class identification process. Ideal spectral signatures were based on 204 unique, ideal samples available from field data. This ground survey information was collected during 2013–14 that corresponded with the 2013–14 MODIS data. Ninety-four other samples were of noncroplands. The 298 samples were grouped according to their unique categories and grouped major rice systems as shown in Fig. 9.3. The samples were chosen to generate ideal spectra signatures that refer to crop intensity, crop type, and cropping systems. Each signature was generated with a group of

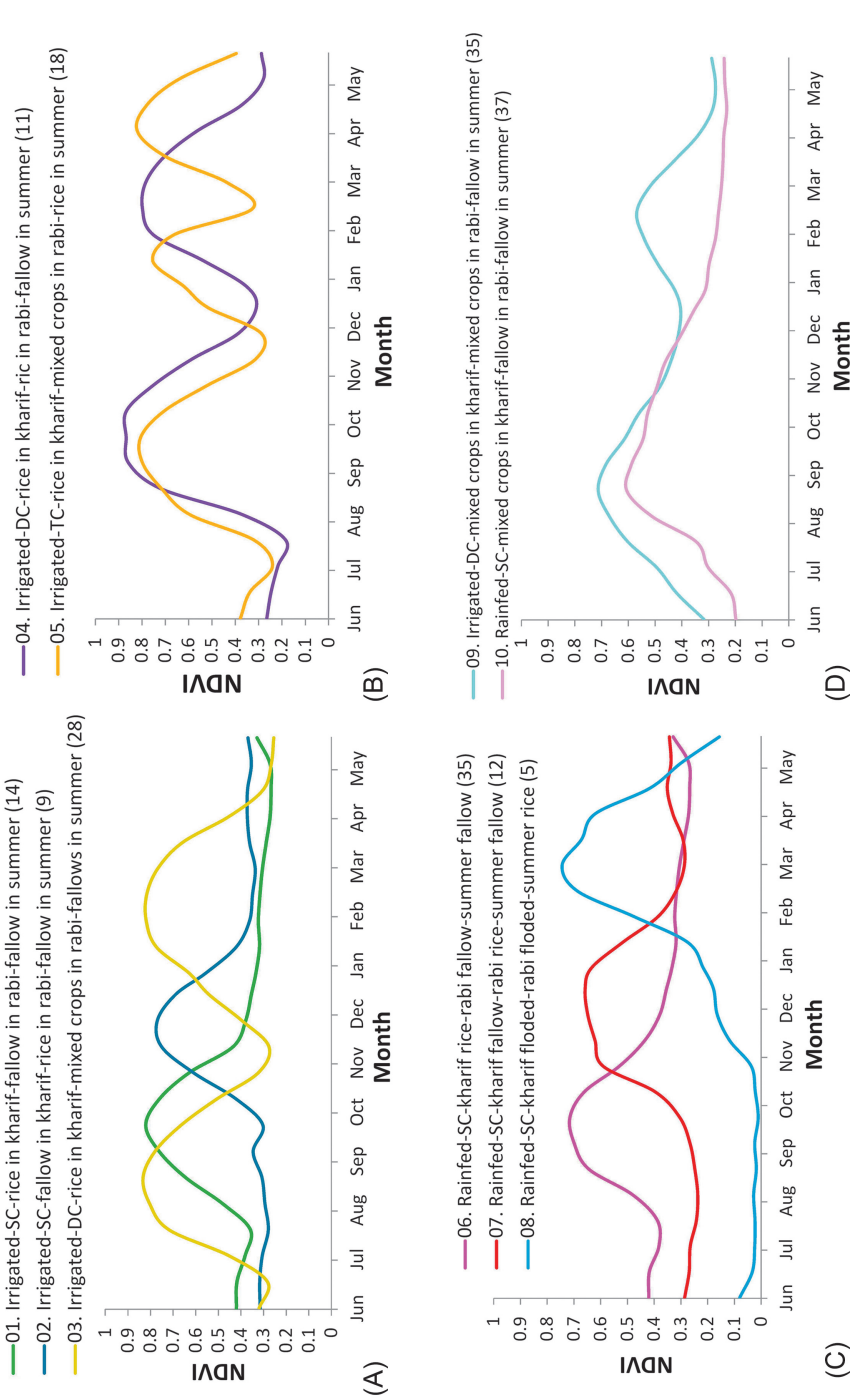

FIG. 9.3 Ideal spectral signatures of 10 cropland classes in South Asia (Gumma et al., 2016). For example, 01. Irrigated, SC, rice in kharif, fallows in rabi, fallows in summer means irrigated single cropland area with rice grown during kharif (June–October), but left fallow during rabi (November–February) and also left fallow in summer (March–May). (A) and (B) are irrigated-rice systems, and (D) is other major croplands.

similar samples. Take, for example, Fig. 9.3A, class 1: the "01. Irrigated-SC –rice in kharif – fallow in rabi-fallow in summer (14)" signature defines irrigated croplands during the kharif season followed by cropland fallows during the rabi season, and the cropland fallows during the summer season. This signature was generated by 14 ground survey samples that were smoothed. Overall, a total of 25 unique cropland classes that are either irrigated or rainfed have differing cropping intensities (e.g., classes 1, 2, 6, 7, 8, and 10 are single crop; classes 3, 4, and 9 are double crop; and class 5 is a triple crop), and distinct phenological cycles.

9.3.4 Mapping Land Use/Land Cover

An overview of the methods (Fig. 9.4) and details are described next. The process began with mapping land use/land cover areas using MODIS 16-day time-series data with spectral matching techniques and field-plot information.

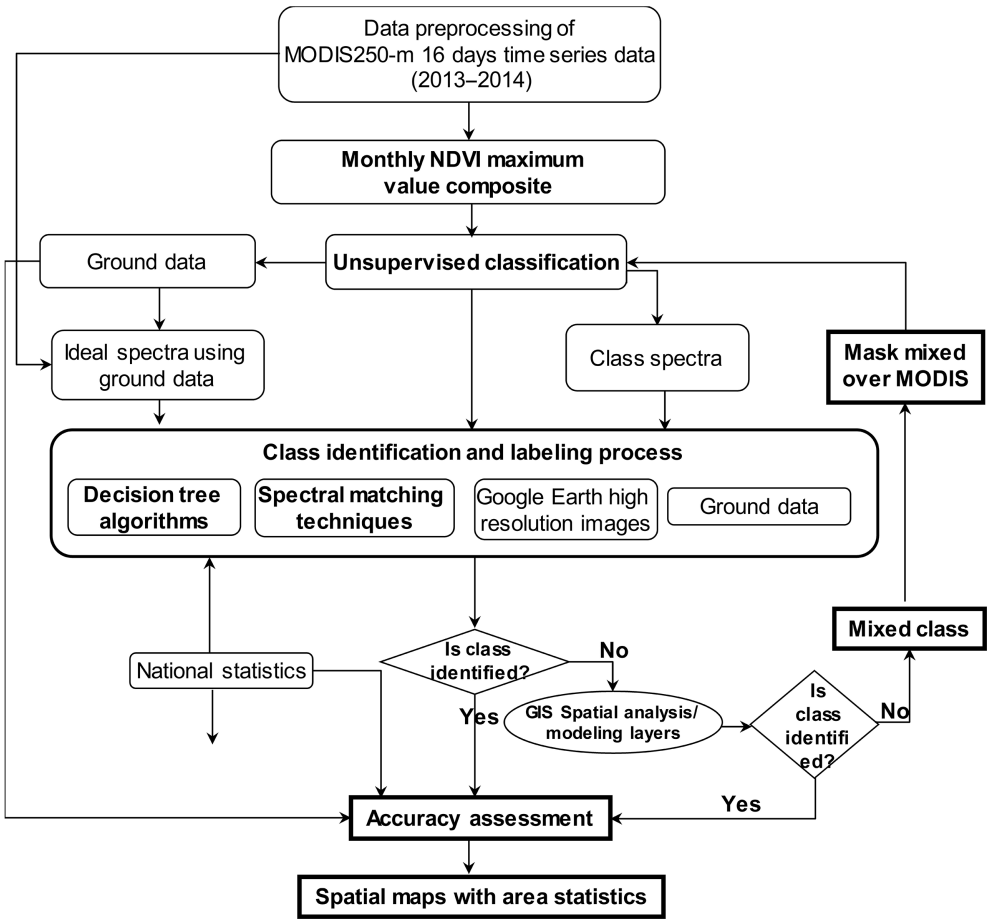

FIG. 9.4 Flow chart describing the analysis process.

MODIS 16-day time-series composite vegetation index images at 250 m resolution were obtained from June 1, 2013 to May 31, 2014 (MOD13Q1 data product). The MOD13Q1 data set are available in the public domain and are pre-calibrated (http://modis-sr.1tdri.org/html). The large scene size and daily overpass rate of MODIS make it attractive for mapping large crop areas, and NDVI images derived from MODIS have high fidelity with biophysical parameters (Huete et al., 2002). The 16-day NDVI images were stacked into a 23-band file for each crop year (two images per month). Monthly maximum value composites were created using 16-day NDVI MODIS data to minimize cloud effects (Holben, 1986).

Unsupervised classification was used to generate initial classes. The unsupervised ISOCLASS cluster algorithm (ISODATA in ERDAS Imagine 2016TM) that was run on the NDVI-MVC generated an initial 100 classes, with a maximum of 100 iterations and a convergence threshold of 0.99. Although ground survey data were available at the time of image classification, unsupervised classification was used to capture the full range of NDVI over a large area. Use of unsupervised techniques is recommended for large areas that cover a wide and unknown range of vegetation types, and where landscape heterogeneity complicates identification of homogeneous training sites (Cihlar, 2000; Biggs et al., 2006; Gumma et al., 2011e). Identification of training sites is particularly problematic for small, heterogeneous irrigated areas.

Land use/land cover classes were identified based on NDVI temporal signatures along with ground survey data. We observed crop growth stages and cropping patterns from temporal signatures, such as (1) onset of cropping season (e.g., monsoon and winter), (2) duration of cropping season (e.g., monsoon and winter), (3) magnitude of crops during different seasons and years (e.g., water-stressed and normal years), and (4) end of cropping season (Gumma et al., 2011a,e).

The process of labeling class identification was done based on spectral matching techniques (SMTs) (Thenkabail et al., 2007b; Gumma et al., 2016). Initially, 160 classes from the unsupervised classification were grouped based on spectral similarity or closeness of class signatures. Each group of classes was matched with ideal spectra signatures and ground survey data and assigned class names (Gumma et al., 2014, 2016). Classes with similar NDVI time-series and land cover were merged into a single class, and classes showing significant mixing, for example, continuous irrigated areas and forest, were masked and reclassified using the same ISOCLASS algorithm. Some continuous irrigated areas mixed with forests in the Western Ghats were separated using a 90 m digital elevation model (DEM) from the Shuttle Radar Topography Mission (SRTM) and an elevation threshold of 630 m, Landsat imagery, and ground survey data through spatial modeling techniques such as overlay matrix, recode, and proximity analysis (Tomlinson, 2003; Gumma et al., 2011d). This resulted in nine classes of LULC. While class aggregation could have been performed statistically using a Euclidean or other distance measure, we employed a user-intensive method that incorporates both ground survey data and high-resolution imagery in order to avoid lumping classes that might be spectrally similar but have distinct land cover. The NDVI of some classes differed in only one or 2 months, which would cause the classes to be merged if an automated similarity index were used.

Classification was done at 250 m spatial resolution. In the present study area, average land holding size is less than a pixel and there are different land use/land cover classes with 250 m × 250 m pixel (6.25 ha). Full pixel areas are not an accurate representation of actual

cropland areas. The cropland fraction was calculated using the methodology described in (Thenkabail et al., 2007b; Gumma et al., 2011a,d, 2015a). Subpixel areas were important when a particular pixel was named as cropland but also contained other land use/land cover classes (grasses, trees, shrubs, etc.).

Ground data points were used to assess the accuracy of the classification results, based on a standard procedure (Jensen, 1996; Congalton and Green, 1999, 2008), to generate an error matrix and accuracy measures for each land use/land cover map. Error matrices and Eq. (9.2) (Farr and Kobrick, 2000) "Cohen's kappa coefficient (κ)" are commonly used for accuracy assessment. For example, these are useful when building models that predict discrete classes or when classifying imagery. κ can be used as a measure of agreement between model predictions and reality (Congalton, 1991a) or to determine if the values contained in an error matrix represent a result significantly better than random (Jensen, 1996). κ is computed as

$$\kappa = \frac{N\sum_{i=1}^{r} x_{ii} - \sum_{i=1}^{r}(x_{i+} \times x_{+i})}{N^2 - \sum_{i=1}^{r}(x_{i+} \times x_{+i})} \tag{9.2}$$

where N is the total number of sites in the matrix, r is the number of rows in the matrix, xii is the number in row i and column i, $x+i$ is the total for row i, and $xi+$ is the total for column i (Jensen, 1996).

9.3.5 Matching Class Spectra With Ideal Spectra to Group Classes Using Spectral Matching Techniques (SMTs)

The initial 160 unsupervised classes (called class spectra) were arranged into a number of groups based on quantitative spectral matching techniques (Homayouni and Roux, 2003; Thenkabail et al., 2007a,b). Fig. 9.3 shows the grouping of some of these classes. This homogeneous class was then matched with ideal spectra (see Fig. 9.3) for preliminary class identification and labeling. Additional verification was conducted using ground data, and high-resolution imagery from Google Earth and GeoCover by overlaying minor (e.g., district) administrative boundaries in the Google Earth application. Mixed classes remained because of the large extent and diverse land use of small holdings. To resolve these mixed classes we used various other sources, such as irrigation command area boundaries, rainfall, district-level statistics, and high-resolution imagery using spatial modeling (Gumma et al., 2014). Some classes did not resolve conclusively, even after using ground survey information and other information previously mentioned. These classes were then subset, reclassified, and reanalyzed following the preceding protocols (Thenkabail et al., 2007b; Gumma et al., 2011a, 2014).

Fig. 9.5 illustrates the group of croplands in kharif-croplands in rabi-fallow in summer classes, which was matched with class 4 (see Fig. 9.2) in ideal spectra signatures. Initially classes were grouped based on decision tree algorithms and spectral similarity. This group of classes was then matched with ideal spectra (Fig. 9.5C) for preliminary class identification and

labeling. Additional verification was conducted using ground survey information data, and high-resolution imagery from Google Earth and GeoCover by overlaying minor (e.g., district) administrative boundaries in the Google Earth application. In Fig. 9.5 initially 14 classes were grouped through decision tree algorithm, and finally 21 classes were closely correlation with ideal spectra class 4.

9.3.6 Subpixel Area Calculations

Full pixel areas (FPAs) are not correct representations of actual areas. For example, in each cropland class there are often thousands or millions of pixels. The proportion of area cropped in each of these thousands or millions of pixels varies significantly, even in a single cropland class. This situation results, for example, if we map all pixels with 50% or more covered in maize crops, because in a maize class, there will be pixels in which the maize proportion varies between 50% and 100%. So to get actual areas, the FPAs need to be multiplied by the cropland area fraction (CAF). The CAF will depend on the percentage of area in a pixel that actually belongs to a class. In the case of the previously discussed maize crop class, the CAF will vary between 0.5 and 1.0. Therefore the FPAs with CAFs of 0.5 will be multiplied by 0.5, FPAs with CAFs of 0.55 will be multiplied by 0.55, and so on. Overall, the actual areas are equivalent to the subpixel areas (SPAs), as shown in previous well-established studies (Thenkabailc et al., 2007). That is, each pixel in each class is assessed for its actual area as follows:

$$\text{SPAs or actual areas} = \text{FPAs}^{*}\,\text{CAFs}$$

Extensive details of this methodology are explained in (Thenkabailc et al., 2007). SPAs or actual area calculations gain greater significance as pixel sizes become coarser. In the present study the MOD13Q1 pixel cover is 250 m per side, and its area is 6.25 ha. So for a pixel for an area only 50% cropped, a FPA-based area calculation per pixel will be 6.25 ha, whereas the SPA or actual area will be 3.125 ha (6.25 ha * 0.5). Thus unless we calculate areas based on SPA, there will be huge discrepancies in actual areas.

9.3.7 Accuracy Assessments

Accuracy assessment was based on a total of 346 independent ground samplings, as described in Section 9.3.2. These data points were not used in class identification and labeling. The accuracy of the classification results, based on (Jensen, 2004), were used to generate an error matrix and accuracy measures for final classification. The columns (x-axis) of an error matrix contain the ground survey data points, and the rows (y-axis) represent the results of the classified rice maps (Congalton, 1991b). The error matrix is a multidimensional table in which the cells contain changes from one class to another. The statistical approach of accuracy assessment consists of different multivariate statistical analyses. A frequently used measure is the Kappa measurement system, which is designed to compare results from different regions or different classifications.

9.4 RESULTS AND DISCUSSIONS

9.4.1 Spatial Distribution of Croplands in Indo-Ganges Basin

The objectives of this study and based on the methods described in above sections, distinct cropland classes of Indo-Ganges basin.

- Identify crop type\dominance in different seasons with a focus on major croplands, including source of irrigation.
- Establish the season in which croplands are cultivated and also establish the season in which croplands are fallow.

Using the preceding focus, we identified and labeled cropland classes in the Indo-Ganges Basin (see Fig. 9.4) based on the methods and approaches discussed throughout Section 9.2. Fig. 9.5 shows the spatial distribution of all the cropland areas in the Indo-Ganges Basin with 19 distinct cropland classes and two other land cover\land use (LCLU); their statistics are provided in Table 9.3.

A total of 21 LULC classes (Fig. 9.6 and Table 9.3) were mapped, showing clear spectral separateability on one or more single dates, and/or one or more multiple dates, and/or over a near-continuous time interval (Thenkabail et al., 2005). The total study area in the Ganges and Indus basins was 216 Mha (Table 9.3), of which there was a high degree of irrigation (see classes 1 through 9 in Fig. 9.6 and Table 9.3).

The LULC name or label *was* based on the predominance of a particular land cover. For example, the name for class 01 is "Irrigated-SW/GW-DC-rice-wheat." The land cover (Thenkabailc et al.) of this class was dominated by rice-wheat (rice during the kharif season and wheat during the rabi season), and the total area of the class was 18.8 Mha, with 90% of the area covered by croplands, 4% by other LULC, 3% by grasses, and 1% by shrubs. The rice area was predominant in Punjab and Haryana during kharif, and wheat was a winter crop. Class 10 was labeled "Rainfed-DC-rice-fallows-jute/rice/mixed crops" since this was an intensely cropped area class that is heavily dependent on rain. At the time of this ground data, 94% of class 10 had cropland that grew rice during the kharif and rabi seasons, with the rest as follows: 3% comprising trees, 1% comprising shrubs, 1% comprising grasses, and 1% comprising water bodies. Since we had several different types of ground data (e.g., cover percentages, digital photos, observations marked on maps and images), we were able to label classes with as close a match with reality as possible, leading to a final set of 21 LULC classes (Fig. 9.6 and Table 9.3).

The FPA of croplands in the Indo-Ganges Basin was 210,482,000 ha, with 175,670,700 (or 90%) being SPAs during kharif.

9.4.2 Spatial Distribution of Irrigated and Rainfed Croplands in the Indo-Ganges Basin

A total area of 114 Mha (FPA) was estimated in the Indus Basin, including all three major classes (i.e., irrigated croplands, rainfed croplands and other LULCs); and a total area of 102 Mha (FPA) was estimated in the Ganges Basin, including trees, shrubs, grass, water bodies, and other LULC classes (Table 9.4). After excluding the area covered by trees, shrubs, grass,

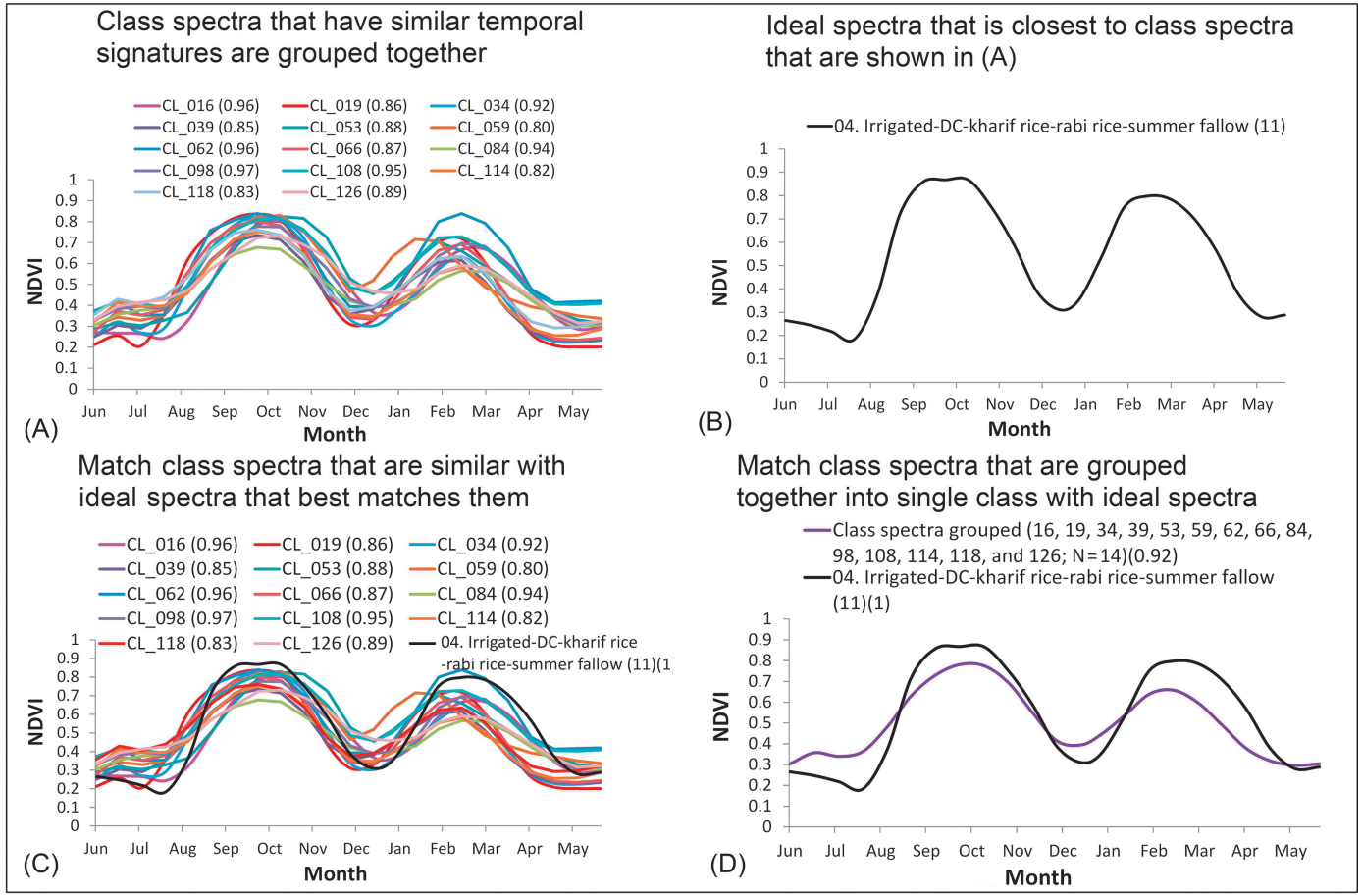

FIG. 9.5 Spectral matching techniques (SMTs) to match class spectra with ideal spectra. The process involves two steps: 1. *Grouping similar class spectra (A)*: For example, of the 160 unsupervised classes, we group all classes that have similar time-series spectral signatures (C and D). (D) For example, classes 16, 34, 53, 62, 66, 84, 98, 108, and 126 group into a single class [they are highly correlated with R-square values of 0.87 or above]. 2. *Finding an ideal spectra that matches closest to class spectra* (B): From the ideal spectral library (Fig. 9.3), we selected an ideal spectra (B) that matches closest to class spectra that are grouped together (A). 3. *Matching group of similar classes with ideal spectra*: For example, the legend "CL_062(0.96)" in (D) means that class 62 has a spectral correlation similarity R-square value (SCS R-square value) of 0.96 with ideal spectra class 4 (04. irrigated, double crop, rice in kharif season, rice in rabi season, and fallow in summer season). So classes 16, 34, 53, 62, 66, 84, 98, 108, and 126 are grouped and given initial label same as ideal spectra class 4. The name is further verified using numerous other ancillary data (e.g., ground data, other published data, high-resolution imagery). 4. *Combining all similar class spectral classes to a single class* (D): Since all the 12 class spectral classes are very highly correlated to one another and in turn they are highly correlated with ideal spectra, the 14 class spectral classes are combined into a single class.

TABLE 9.3 LULC Areas in Indo-Ganges River Basin With Irrigation Source

Land Use/Land Cover	Indus (FPA) ('000 ha)	Ganges (FPA) ('000 ha)	Sample	TREE (%)	SHRUBS (%)	GRASS (%)	Water Bodies (%)	Other LULC (%)	Croplands (%)	Indus (King et al., 2003) ('000 ha)	Ganges (King et al., 2003) ('000 ha)
01. Irrigated-SW/GW-DC-rice-wheat	7983	12,920	31	2	1	3	0	4	90	7208	11,666
02. Irrigated-SW/GW-DC-rice-rice	3853	5901	47	3	1	1	1	0	94	3604	5520
03. Irrigated-SW-DC-sugarcane/rice-rice/plantations (20%)	173	917	36	2	1	0	0	1	97	167	885
04. Irrigated-SW-DC-beans/cotton-wheat	1187	8872	32	1	1	6	0	1	90	1072	8010
05. Irrigated-GW-DC-millet/sorghum/potato-wheat/mustard	6315	14,644	55	1	1	3	0	1	94	5929	13,748
06. Irrigated-DC-fallows/pulses-rice-fallow	158	259	38	3	1	2	0	1	92	146	240
07. Irrigated-GW-DC-rice-maize/chickpea	155	2640	3	4	1	2	0	2	92	142	2420
08. Irrigated-TC-rice-mixed crops-mixed crops	112	2260	39	4	1	1	0	0	94	105	2122
09. Irrigated-SW-DC-cotton/chili/maize-fallow/pulses	7	84	29	1	1	1	0	4	93	7	78
10. Rainfed-DC-rice-fallows-jute/rice/mixed crops	125	2320	30	3	1	1	1	0	94	117	2171
11. Rainfed-SC-rice-fallow/pulses	7	59	7	1	1	1	1	2	94	7	55

TABLE 9.3 LULC Areas in Indo-Ganges River Basin With Irrigation Source—cont'd

Land Use/Land Cover	Indus (FPA) ('000 ha)	Ganges (FPA) ('000 ha)	Sample	TREE (%)	SHRUBS (%)	GRASS (%)	Water Bodies (%)	Other LULC (%)	Croplands (%)	Indus (King et al., 2003) ('000 ha)	Ganges (King et al., 2003) ('000 ha)
12. Rainfed-DC-millets-chickpea/fallows	745	999	5	0	3	0	7	0	90	668	896
13. Rainfed-SC-cotton/pigeonpea/mixed crops	421	3024	178	1	2	4	0	5	89	374	2682
14. Rainfed-SC-groundnut/millets/sorghum	356	204	68	1	1	2	0	3	93	330	189
15. Rainfed-SC-pigeonpea/mixed crops	93	1432	35	2	1	2	0	1	93	86	1337
16. Rainfed-SC-millet-fallows/mixed crops-	3658	3483	11	0	2	9	0	1	88	3222	3068
17. Rainfed-SC-fallow-chickpea-	18	28	21	1	1	1	0	9	89	16	25
18. Rainfed-SC-millets/fallows-LS	5140	7	6	1	1	12	0	5	81	4164	5
19. Rainfed-SC-mixed crops/plantations	1155	1624	36	8	3	2	0	0	86	997	1402
20. Shrub lands/trees/rainfed-mixedcrops30%	7	187	9	2	41	8	1	0	48	3	90
21. Other LULC	82,506	40,240	129	27	20	19	5	16	13	10,635	5187

*The table shows full-pixel area (FPA), crop area fraction (CAF), and subpixel area (King et al., 2003) or actual area. SPA = FPA * CAF.*

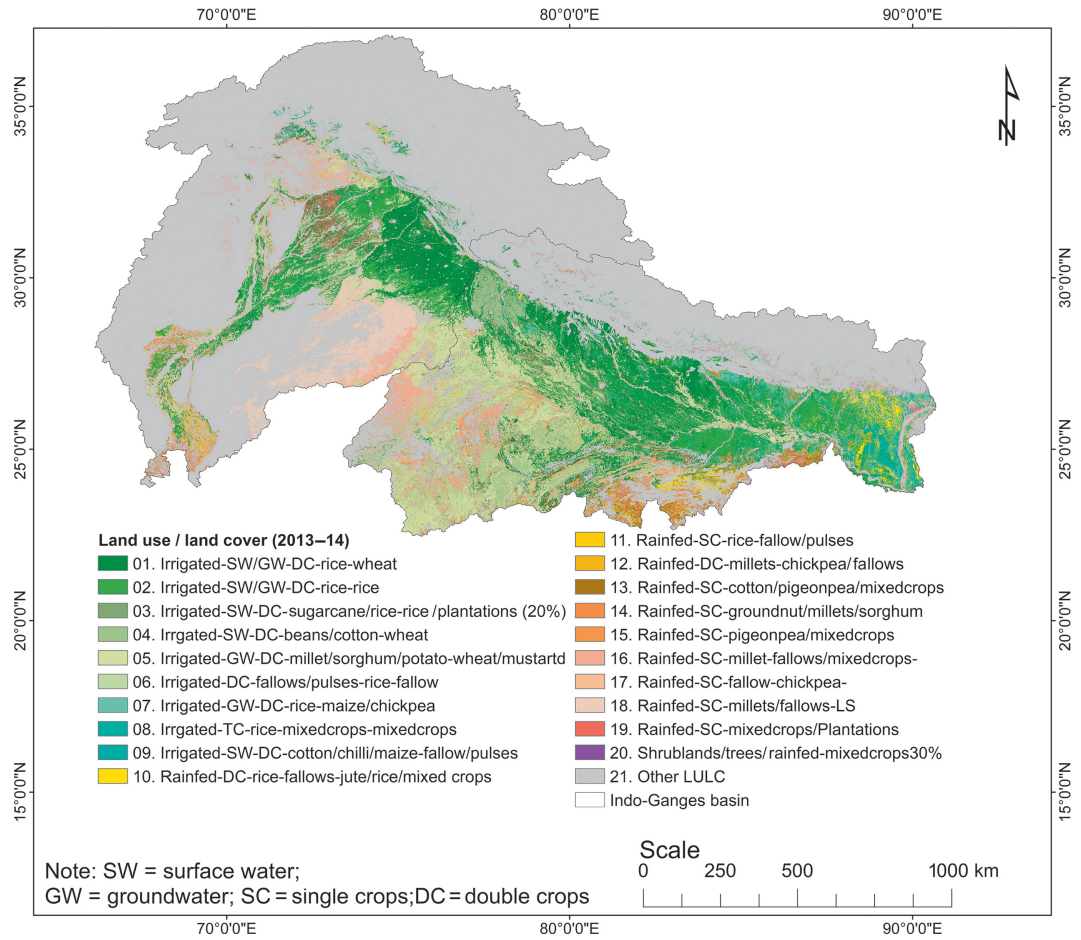

FIG. 9.6 Spatial distribution of croplands and their characteristics in the Indo-Ganges River Basin. The 21 classes show cropland classes that have single or double or triple cropping and where rice or other crops dominate. The classes also show seasonality of cropping and when croplands are left fallow.

water bodies, and other LULC classes, in all three major classes, a total area of 28.4 Mha was estimated (i.e., all the area covered by croplands in the Indus Basin and 56.6 Mha in the Ganges Basin).

A total area of 19.9 Mha (FPA) in the Indus Basin and a total area of 48.5 Mha (FPA) in the Ganges Basin was estimated with 310 samples, in which trees comprised 2%, shrubs comprised 1%, grass comprised 2%, water bodies comprised 0%, other LULC classes comprised 2%, and cropland comprised 93%. Excluding tree, shrubs, grass, water bodies, and other LULC classes, the exact area of irrigated croplands was 18.4 Mha in the Indus Basin and 44.7 Mha in the Ganges Basin (Table 9.4).

A total area of 11.7 Mha (FPA) in the Indus Basin and a total area of 13.4 Mha (FPA) in the Ganges Basin was estimated with 406 samples, in which trees comprised 2%, shrubs

TABLE 9.4 Irrigated Areas vs. Rainfed Cropland Area in Indo-Ganges River Basin With Irrigation Source

	Indus (FPA) ('000 ha)	Ganges (FPA) ('000 ha)	Sample	TREE (%)	SHRUBS (%)	GRASS (%)	Water Bodies (%)	Other LULC (%)	Croplands (%)	Indus (King et al., 2003) ('000 ha)	Ganges (King et al., 2003) ('000 ha)
01. Irrigated-croplands	19,943	48,498	310	2	1	2	0	2	93	18,379	44,689
02. Rainfed-croplands	11,725	13,367	406	2	6	3	1	2	86	9984	11,921
03. Other LULC	82,506	40,240	129	27	20	19	5	16	13	10,635	5187

*The table shows full-pixel area (FPA), crop area fraction (CAF), and subpixel area (King et al., 2003) or actual area. SPA = FPA * CAF.*

comprised 6%, grass comprised 3%, water bodies comprised 1%, other LULC classes comprised 2%, and cropland comprised 86%. Excluding trees, shrubs, grass, water bodies, and other LULC classes, the exact area of rainfed croplands in the Indus Basin was 9.98 Mha and 11.9 Mha in the Ganges Basin.

A total area of 82.5 Mha (FPA) in the Indus Basin and a total area of 40.2 Mha (FPA) in the Ganges Basin was estimated with 129 samples, in which trees comprised 27%, shrubs comprised 20%, grass comprised 19%, water bodies comprised 5%, other LULC classes comprise d16%, and cropland comprised 13%. Excluding tree, shrubs, grass, water bodies, and other LULC classes, the exact area of croplands occurring in other LULC classes was 10.6 Mha in the Indus Basin and 5.2 Mha in the Ganges Basin.

An accuracy assessment was done for the final LULC map in the Indo-Ganges River Basin, and three classes were classified using ground points. A total of 209 samples, comprising 101 and 36 columns, were classed as irrigated croplands, rainfed croplands, and noncroplands (other LULCs). Based on 346 reference totals and 346 classified totals, a total of 317 correct pixels occurred in classification, with an overall classification accuracy of 91.62%; thus an overall *kappa Statistics assessment* was done with 0.84 accuracy.

A total of 218 pixels were classified for the irrigated croplands class, in which 200 pixels were classified as irrigated croplands, 13 pixels were classified as rainfed croplands, and 5 pixels were classified as noncroplands (other LULCs), with an overall reference total of 209 pixels. A total of 200 pixels were correctly classified for irrigated croplands, with a producer's accuracy of 95% and a user's accuracy of 92% and an overall kappa coefficient of 79%.

A total of 93 pixels were classified for the rainfed croplands class, in which 7 pixels were classified as irrigated croplands, 86 pixels as rainfed croplands, and zero pixels as noncroplands (other LULCs), with an overall reference total of 101 pixels. A total of 86 pixels were correctly classified for rain-fed croplands, with 85% producer's accuracy and 92% user's accuracy and an overall kappa coefficient of 89%.

A total of 36 pixels were classified for the noncroplands (other LULCs) class, in which 2 pixels were classified as irrigated croplands, 2 pixels as rainfed croplands, and 31 pixels as noncroplands (other LULCs), with an overall reference total of 36 pixels. A total of 31 pixels were correctly classified for noncroplands (other LULCs), with 86% producer's accuracy and 89% user's accuracy and an overall kappa coefficient of 87%.

9.4.3 Class Signatures and Onset-Peak-Senescence-Duration of Crops

The class signatures of NDVI (CS-NDVI) are unique spectral properties of a class that can be mapped using NDVI time-series data of a class (see Fig. 9.5A). It is not possible to have spectral signatures when single-date images or images with a few dates are used, as is often the case with LULC studies. Since near-continuous MODIS data were used in this study, a unique set of LULC class signatures were possible (see Fig. 9.3) for classes mapped in Fig. 9.6.

The threshold NDVIs and NDVI signatures over time help us determine (see Table 9.3 and Figs. 9.6 and 9.7) (1) onset of a cropping seasons (e.g., kharif and rabi), (2) duration of the cropping seasons (e.g., for kharif and rabi), (3) magnitude of the crops during different seasons and years (e.g., drought versus normal years), and (4) end of cropping season (senescence). In order to illustrate these possibilities, the MODIS CS-NDVI signatures are presented and

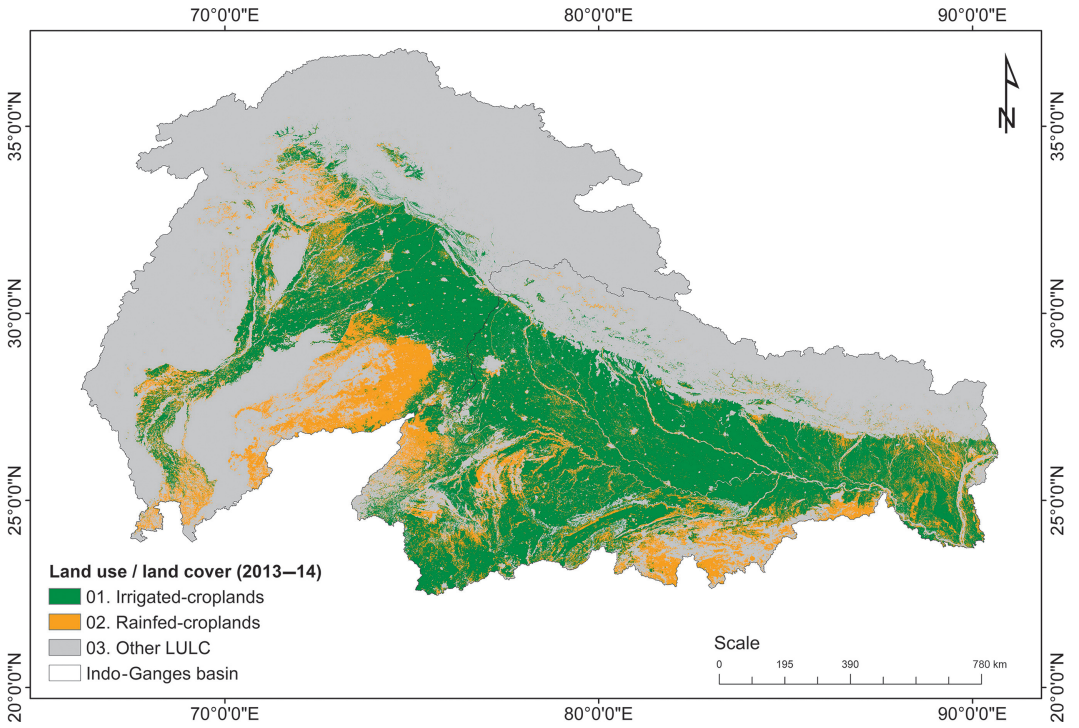

FIG. 9.7 Spatial distribution of irrigated and rainfed croplands in Indo-Ganges River Basin.

discussed for a set of distinct classes (Fig. 9.3) and thematically similar classes (see Fig. 9.5A). The NDVI of irrigated classes never falls below 0.7 on the peak growth stage during the kharif season (see Fig. 5A).

9.4.4 Accuracies and Errors

Accuracy assessment was performed on two independent classification products as shown in Figs. 9.6 and 9.7. Accuracies of the classes were established based on 346 ground sample data (see Tables 9.5 and 9.6), which provided an overall accuracy of 71% with a kappa coefficient of 0.73. The user's and producer's accuracies of most classes were above 80%. Even when they were somewhat lower, the class mix was mainly among cropland classes.

9.4.5 Comparison With District Wise Cropland Statistics

Fig. 9.6 illustrates the spatial extent of rice-wheat growing areas (see also Table 9.6) derived from MOD13Q1 time-series data with spectral matching techniques. To assess how well the spatial extent of rice-wheat (rice during kharif, wheat during rabi) were estimated, we correlated district wise statistics of rice areas obtained from national statistics, resulting in a R2 value of 0.84.

TABLE 9.5 Accuracy Assessment Using Error Matrix (Land Use/Land Cover Classification)

	CL_01	CL_02	CL_03	CL_04	CL_05	CL_06	CL_07	CL_08	CL_09	CL_10	CL_11	CL_12	CL_13	CL_14	CL_15	CL_16	CL_17	CL_18	CL_19	CL_20	CL_21	Row Total	Number Correct	Producer's Accuracy (%)	User's Accuracy (%)	Kappa
CL_01	20	5	0	2	2	0	0	0	0	0	2	0	0	0	0	1	0	0	0	0	3	35	20	74%	57%	54%
CL_02	0	17	1	0	0	0	2	3	0	1	0	0	0	0	0	0	0	0	0	0	1	25	17	59%	68%	65%
CL_03	1	0	8	0	0	0	0	0	0	0	0	0	0	0	0	0	0	0	0	0	0	9	8	80%	89%	89%
CL_04	0	0	0	19	2	0	0	4	0	0	4	0	5	0	0	1	0	0	0	0	0	35	19	79%	54%	51%
CL_05	3	0	0	2	45	0	0	0	0	0	1	6	0	0	0	1	0	0	0	0	0	58	45	83%	78%	73%
CL_06	3	0	0	0	0	13	0	0	0	0	0	0	0	0	0	0	0	0	0	0	1	17	13	76%	76%	75%
CL_07	0	2	1	0	0	0	5	0	0	0	0	0	0	0	0	0	0	0	0	0	0	8	5	71%	63%	62%
CL_08	0	2	0	0	1	4	0	14	0	1	0	0	0	0	0	0	0	0	0	0	0	22	14	54%	64%	61%
CL_09	0	0	0	0	0	0	0	2	6	0	0	0	0	0	0	0	0	0	0	0	0	8	6	100%	75%	75%
CL_10	0	2	0	0	1	0	0	2	0	8	0	0	0	0	0	0	0	0	0	0	0	13	8	80%	62%	60%
CL_11	0	0	0	0	0	0	0	0	0	0	7	0	0	0	0	0	0	0	0	0	0	7	7	50%	100%	100%
CL_12	0	0	0	0	0	0	0	0	0	0	0	2	0	0	0	0	0	0	0	0	0	2	2	25%	100%	100%
CL_13	0	0	0	0	0	0	0	0	0	0	0	0	5	0	0	0	0	0	0	0	0	5	5	50%	100%	100%
CL_14	0	0	0	0	0	0	0	0	0	0	0	0	0	8	2	0	0	0	0	0	0	10	8	89%	80%	79%
CL_15	0	0	0	0	0	0	0	0	0	0	0	0	0	1	7	1	0	0	0	0	0	9	7	78%	78%	77%
CL_16	0	0	0	0	0	0	0	1	0	0	0	0	0	0	0	9	0	0	0	0	0	10	9	69%	90%	90%
CL_17	0	0	0	0	0	0	0	0	0	0	0	0	0	0	0	0	4	0	0	0	0	4	4	67%	100%	100%
CL_18	0	0	0	0	0	0	0	0	0	0	0	0	0	0	0	0	2	17	0	0	0	19	17	89%	89%	89%
CL_19	0	0	0	0	0	0	0	0	0	0	0	0	0	0	0	0	0	0	13	0	0	13	13	76%	100%	100%
CL_20	0	0	0	0	0	0	0	0	0	0	0	0	0	0	0	0	0	0	2	2	0	4	2	100%	50%	50%
CL_21	0	1	0	1	3	0	0	0	0	0	0	0	0	0	0	0	0	2	2	0	24	33	24	83%	73%	70%
Column Total	27	29	10	24	54	17	7	26	6	10	14	8	10	9	9	13	6	19	17	2	29	346	253			

Overall Kappa Statistics = 0.7097

Overall Classification Accuracy = 73.12%

TABLE 9.6 LULC Areas in Indo-Ganges River Basin With Irrigation Source

Land Use/ Land Cover	01. Irrigated-Croplands	02. Rainfed-Croplands	03. Noncroplands (Other LULC)	Reference Totals	Classified Totals	Number Correct	Producers Accuracy	Users Accuracy	Kappa
01. Irrigated-croplands	200	13	5	209	218	200	96%	92%	79%
02. Rainfed-croplands	7	86	0	101	93	86	85%	92%	89%
03. Noncroplands (Other LULC)	2	2	31	36	35	31	86%	89%	87%
Column Total	209	101	36	346	346	317			
Overall Classification Accuracy = 91.62%				Overall Kappa Statistics = 0.8420					

*The table shows full-pixel area (FPA), crop area fraction (CAF), and subpixel area (King et al., 2003) or actual area. SPA = FPA * CAF.*

9.4.6 Discussion of Methods

Mapping cropland areas is useful for understanding and determining options for producing more food, which is critical for ensuring global food security. Greater food production for a growing population requires more land. Since cropland expansion is not feasible and has costly environmental and ecological impacts (Tilman, 1999; Tilman et al., 2002; Thenkabail et al., 2012; Kuemmerle et al., 2013), cropland intensification by cultivating existing fallow croplands is a possible option. This study investigated the Indo-Ganges Basin extensively using MODIS 250 m NDVI time-series data to arrive at cropland classes (see Fig. 9.6) from which two cropland classes (irrigated croplands and rainfed croplands) (see Fig. 9.7) were identified, with a total cropland area of about 84 Mha (see Table 9.2 and Fig. 9.6) as fallow cropland during the rabi season.

The present research used MOD13Q1.5 temporal data to identify major croplands and irrigated areas across the Indo-Ganges Basin. MODIS captures imagery on a daily basis. The 16-day composites from the daily acquisitions combine to make a time-series data set over a crop year or a calendar year. This type of data set provides temporal profiles of crop-growing locations to identify the start of a season, the peak growth stage, and the harvest date during each season. The value of NDVI as a function of time also helps in identifying the type of crop in an eco-region based on certain peak thresholds for that crop. This study applied a spectral matching technique that is found to be ideal in mapping irrigated areas (Thenkabail et al., 2007a) and mapping rice areas (Gumma et al., 2011a). Mapping the spatial distribution of rice fallows using a MODIS 250 m 16-day time-series and ground survey information with spectral matching techniques represents a significant, new advancement in the use of this technology. The advantage of using a spectral matching technique in this study is that we were able to selectively use the ideal spectral profiles of rice during the rainy season. The rainfed rice spectral class varies from 0.25 to 0.70 for purely rainfed rice and 0.25 to 0.85 for irrigated rice during the rainy season. The qualitative (shape) difference between ideal spectra and class spectra is narrow and represents the fallow lands accurately.

Some discrepancies were also found during the comparison between national statistics and MODIS-derived cropland areas. The mismatch occurred in the eastern part of India, where there was misclassification with irrigated areas due to similar growing conditions during the cropping season. Most of these areas were corrected using rainfall data and spatial modeling techniques.

Cropped area fractions (the proportion of an irrigated/rice area in a pixel) were assigned based on land use proportions in each class to better calibrate the MODIS pixel area to the real irrigated/rice area. Also, this method relies on ground survey information that is a truly representative sample of the fragmented rice systems. Higher resolution imagery could be used to provide a more accurate estimate of pure classes, but wall-to-wall coverage, repeat coverage during a crop's growing period, costs, and massive processing are all major issues that are hard to surmount for areas as large as the Indo-Ganges Basin. Results clearly show that present methods and MODIS time-series data have many advantages, such as capturing a large-scale cropping pattern. But to minimize errors, additional research will be needed using multi-sensor images with advanced fusion techniques (Gumma et al., 2011c).

The areas of the Indo-Ganges Basin where rice predominates are usually located in zones that receive high rainfall during the monsoon season (Satyanarayana et al., 1997; Ali et al., 2014).

Following the rice season, enough soil moisture may remain to facilitate the growth of short-duration crops. While an important reason for fallowing these lands is the scarcity of water during the rabi season, short-season crops and especially legumes, which can biologically fix N, have a higher chance of success. Accurate up-to-date spatial distribution of rice fallows and statistics are important to guide breeders, agronomists, and policymakers toward promoting short-duration crops in this region. Research is required to provide information on systems' aspects, such as the amount of water available for soil, the incidence of unseasonal rainfall, and other agronomic factors.

Cropping systems were mapped in the Indo-Ganges Basin for the years 2013–14, accounting for a total area of 85 Mha. The source of water and the crop intensity were also considered in the classification of the land cover. The net irrigated cropland area derived from MODIS was 63 Mha (18.3 Mha in the Indus River Basin and 44.7 Mha in the Ganges River Basin), and the rainfed cropland area was 21.9 Mha (10 Mha in the Indus River Basin and 11.9 Mha in the Ganges River Basin).

9.5 CONCLUSIONS

This study espoused a vegetation phenological approach using MODIS 250 m time-series data to map agriculture croplands in the Indo-Ganges River Basin. Annual average NDVI and timing of onset of greenness allowed separation of groundwater from surface water. The specific land use categories separated were as follows. The time-series NDVI phenological signatures were distinctly different in the Indo-Ganges Basin in terms of (1) spatial distribution of major croplands, (2) use of surface water for irrigation of continuous crops, and (3) use of groundwater to irrigate crops. Overall, 19 cropland classes, rice fallows 2.3 Mha (see Fig. 9.6 and Table 9.2) of subpixel areas (SPAs) or actual areas during kharif. The overall accuracy of cropland mapping was 73% with a kappa coefficient of 0.71%. The irrigated versus rainfed croplands (with rice as kharif crop) showed producer's accuracies between 96% and 85% and a user's accuracy of 92%.

References

Aitken, B., 1992. Seven Sacred Rivers. Penguin Books India, New Delhi.

Ali, M., Ghosh, P., Hazra, K., 2014. Resource conservation technologies in rice fallow. In: Ghosh, P.K., Kumar, N., Venkatesh, M.S., Hazra, K.K., Nadarajan, N. (Eds.), Resource Conservation Technology in Pulses. Scientific Publishers, ISBN: 978-81-7233-885-5, pp. 83–88. Chapter 7.

Badhwar, G.D., 1984. Automatic corn-soybean classification using landsat MSS data. I. Near-harvest crop proportion estimation. Remote Sens. Environ. 14, 15–29.

Bhutta, M.N., Van der Velde, E.J., 1992. Equity of water distribution along secondary canals in Punjab, Pakistan. Irrig. Drain. Syst. 6 (2), 161–177.

Biggs, T.W., Thenkabail, P.S., Gumma, M.K., Scott, C.A., Parthasaradhi, G.R., Turral, H.N., 2006. Irrigated area mapping in heterogeneous landscapes with MODIS time series, ground truth and census data, Krishna Basin, India. Int. J. Remote Sens. 27, 4245–4266.

Biradar, C.M., Thenkabail, P.S., Noojipady, P., Li, Y., Dheeravath, V., Turral, H., Velpuri, M., Gumma, M.K., Gangalakunta, O.R.P., Cai, X.L., Xiao, X., Schull, M.A., Alankara, R.D., Gunasinghe, S., Mohideen, S., 2009. A global map of rainfed cropland areas (GMRCA) at the end of last millennium using remote sensing. Int. J. Appl. Earth Obs. Geoinf. 11, 114–129.

Casanova, D., Epema, G., Goudriaan, J., 1998. Monitoring rice reflectance at field level for estimating biomass and LAI. Field Crop Res. 55, 83–92.
Chapin III, F.S., Zavaleta, E.S., Eviner, V.T., Naylor, R.L., Vitousek, P.M., Reynolds, H.L., Hooper, D.U., Lavorel, S., Sala, O.E., Hobbie, S.E., Mack, M.C., 2000. Consequences of changing biodiversity. Nature 405 (6783), 234.
Cihlar, J., 2000. Land cover mapping of large areas from satellites: status and research priorities. Int. J. Remote Sens. 21, 1093–1114.
Congalton, R.G., 1991a. Remote sensing and geographic information system data integration: error sources and. Photogramm. Eng. Remote Sens. 57, 677–687.
Congalton, R.G., 1991b. A review of assessing the accuracy of classifications of remotely sensed data. Remote Sens. Environ. 37, 35–46.
Congalton, R., Green, K., 1999. Assessing the Accuracy of Remotely Sensed Data: Principles and Practices. Lewis, New York.
Congalton, R.G., Green, K., 2008. Assessing the Accuracy of Remotely Sensed Data: Principles and Practices. CRC Press.
De Fries, R.S., Hansen, M., Townshend, J.R., Sohlberg, R., 1998. Global land cover classifications at 8 km spatial resolution: the use of training data derived from Landsat imagery in decision tree classifiers. Int. J. Remote Sens. 19 (16), 3141–3168.
Dheeravath, V., Thenkabail, P.S., Chandrakantha, G., Noojipady, P., Reddy, G.P.O., Biradar, C.M., Gumma, M.K., Velpuri, M., 2010. Irrigated areas of India derived using MODIS 500 m time series for the years 2001–2003. ISPRS J. Photogramm. Remote Sens. 65, 42–59.
ERDAS, 2003. ERDAS Field Guide. vol. 1. October 2003.
FAO, 2003. Water Resources Research Institute/FAO. In: 29 (Ed.).
Farr, T.G., Kobrick, M., 2000. Shuttle radar topography mission produces a wealth of data. EOS Trans. 81, 583–585.
Gaur, A., Biggs, T.W., Gumma, M.K., Parthasaradhi, G., Turral, H., 2008. Water scarcity effects on equitable water distribution and land use in major irrigation project – a case study in India. J. Irrig. Drain. Eng. 134 (1), 26–35.
Gray, J., Friedl, M., Frolking, S., Ramankutty, N., Nelson, A., Gumma, M., 2014. Mapping Asian cropping intensity with MODIS. IEEE J. Sel. Top. Appl. Earth Observ. Remote Sens. 7, 3373–3379.
Gumma, M.K., 2008. Methods and approaches for irrigated area mapping at various spatial resolutions using AVHRR, MODIS and LANDSAT ETM+ data for the Krishna river basin, India. PhD Thesis, JNTU, Hyderabad, Telangana.http://publications.iwmi.org/pdf/H042567.pdf. (Accessed 3 July 2017).
Gumma, M.K., Andrew, N., Thenkabail, P.S., Amrendra, N.S., 2011a. Mapping rice areas of South Asia using MODIS multitemporal data. J. Appl. Remote. Sens. 5, 053547.
Gumma, M.K., Gauchan, D., Nelson, A., Pandey, S., Rala, A., 2011b. Temporal changes in rice-growing area and their impact on livelihood over a decade: a case study of Nepal. Agric. Ecosyst. Environ. 142, 382–392.
Gumma, M.K., Thenkabail, P.S., Hideto, F., Nelson, A., Dheeravath, V., Busia, D., Rala, A., 2011c. Mapping irrigated areas of Ghana using fusion of 30 m and 250 m resolution remote-sensing data. Remote Sens. 3, 816–835.
Gumma, M.K., Thenkabail, P.S., Muralikrishna, I.V., Velpuri, M.N., Gangadhararao, P.T., Dheeravath, V., Biradar, C.M., Acharya Nalan, S., Gaur, A., 2011d. Changes in agricultural cropland areas between a water-surplus year and a water-deficit year impacting food security, determined using MODIS 250 m time-series data and spectral matching techniques, in the Krishna River basin (India). Int. J. Remote Sens. 32, 3495–3520.
Gumma, M.K., Thenkabail, P.S., Nelson, A., 2011e. Mapping irrigated areas using MODIS 250 meter time-series data: a study on Krishna River basin (India). Water 3, 113–131.
Gumma, M.K., Thenkabail, P.S., Maunahan, A., Islam, S., Nelson, A., 2014. Mapping seasonal rice cropland extent and area in the high cropping intensity environment of Bangladesh using MODIS 500m data for the year 2010. ISPRS J. Photogramm. Remote Sens. 91, 98–113.
Gumma, M.K., Kajisa, K., Mohammed, I.A., Whitbread, A.M., Nelson, A., Rala, A., Palanisami, K., 2015a. Temporal change in land use by irrigation source in Tamil Nadu and management implications. Environ. Monit. Assess. 187, 1–17.
Gumma, M.K., Mohanty, S., Nelson, A., Arnel, R., Mohammed, I.A., Das, S.R., 2015b. Remote sensing based change analysis of rice environments in Odisha, India. J. Environ. Manag. 148, 31–41.
Gumma, M.K., Thenkabail, P.S., Teluguntla, P., Rao, M.N., Mohammed, I.A., Whitbread, A.M., 2016. Mapping rice-fallow cropland areas for short-season grain legumes intensification in South Asia using MODIS 250 m time-series data. Int. J. Digit. Earth 9, 981–1003.

Hao, Z., Hao, F., Singh, V.P., 2016. A general framework for multivariate multi-index drought prediction based on multivariate ensemble streamflow prediction (MESP). J. Hydrol. 539, 1–10.
Holben, B.N., 1986. Characteristics of maximum-value composite images from temporal AVHRR data. Int. J. Remote Sens. 7, 417–1434.
Homayouni, S., Roux, M., 2003. Material mapping from hyperspectral images using spectral matching in urban area. In: Landgrebe, P. (Ed.), IEEE Workshop in honour of Prof. Landgrebe, Washington DC, USA, October 2003.
Huete, A., Didan, K., Miura, T., Rodriguez, E.P., Gao, X., Ferreira, L.G., 2002. Overview of the radiometric and biophysical performance of the MODIS vegetation indices. Remote Sens. Environ. 83, 195–213.
Ilich, N., 1996. Ganges River Basin Water Allocation Modelling Study. Consultant Report to the World Bank, Calgary.
Jensen, J.R., 1996. Introductory Digital Image Processing: A Remote Sensing Perspective. Prentice Hall, Upper Saddle, NJ.
Jensen, J.R., 2004. Introductory Digital Image Processing: A Remote Sensing Perspectivee, third ed. Prentice Hall, Upper Saddle River, NJ. 544 p.
Khan, A.R., 1999. An analysis of surface water resources and water delivery systems in the Indus Basin. International Water Management Institute (IWMI), Lahore, Pakistan.
King, M.D., Closs, J., Spangler, S., 2003. EOS Data Products Handbook Version 1. NASA Goddard Space Flight Center, Greenbelt, MD.
Kuemmerle, T., Erb, K., Meyfroidt, P., Müller, D., Verburg, P.H., Estel, S., Haberl, H., Hostert, P., Jepsen, M.R., Kastner, T., 2013. Challenges and opportunities in mapping land use intensity globally. Curr. Opin. Environ. Sustain. 5, 484–493.
Li, Z., Hao, Z., Shi, X., Déry, S.J., Li, J., Chen, S., Li, Y., 2016. An agricultural drought index to incorporate the irrigation process and reservoir operations: a case study in the Tarim River basin. Glob. Planet. Chang. 143, 10–20.
Loveland, T.R., Reed, B.C., Brown, J.F., Ohlen, D.O., Zhu, Z., Yang, L.W., Merchant, J.W., 2000. Development of a global land cover characteristics database and IGBP DISCover from 1 km AVHRR data. Int. J. Remote Sens. 21 (6–7), 1303–1330.
Meadows, P., 1999. The Indus River: Biodiversity, Resources, Humankind. Oxford University Press for the Linnean Society of London, ISBN: 0195779053, p. 441.
Olsson, P.-O., Lindström, J., Eklundh, L., 2016. Near real-time monitoring of insect induced defoliation in subalpine birch forests with MODIS derived NDVI. Remote Sens. Environ. 181, 42–53.
Penner, J.E., Charlson, R.J., Schwartz, S.E., Hales, J.M., Laulainen, N.S., Travis, L., Leifer, R., Novakov, T., Ogren, J., Radke, L.F., 1994. Quantifying and minimizing uncertainty of climate forcing by anthropogenic aerosols. Bull. Am. Meteorol. Soc. 75 (3), 375–400.
Pittman, K., Hansen, M.C., Becker-Reshef, I., Potapov, P.V., Justice, C.O., 2010. Estimating global cropland extent with multi-year MODIS data. Remote Sens. 2, 1844–1863.
Salmon, J.M., Friedl, M.A., Frolking, S., Wisser, D., Douglas, E.M., 2015. Global rain-fed, irrigated, and paddy croplands: a new high resolution map derived from remote sensing, crop inventories and climate data. Int. J. Appl. Earth Obs. Geoinf. 38, 321–334.
Satyanarayana, A., Seenaiah, P., Sudhakara Babu, K., Prasada Rao, M., 1997. Extending pulses area and production in rice fallow. In: Asthana, A.N., Ali, M. (Eds.), Recent Advances in Pulses Research. Indian Society of Pulses Research and Development, Indian Institute of Pulses Research, Kanpur, India, pp. 569–580.
See, L., Fritz, S., You, L., Ramankutty, N., Herrero, M., Justice, C., Becker-Reshef, I., Thornton, P., Erb, K., Gong, P., 2015. Improved global cropland data as an essential ingredient for food security. Glob. Food Secur. 4, 37–45.
Singh, A., 1989. Review article digital change detection techniques using remotely-sensed data. Int. J. Remote Sens. 10, 989–1003.
Skole, D.L., 2004. Geography as a great intellectual melting pot and the preeminent interdisciplinary environmental discipline. Ann. Assoc. Am. Geogr. 94 (4), 739–743.
Thenkabail, P.S., Stucky, N., Griscom, B.W., Ashton, M.S., Diels, J., Van Der Meer, B., Enclona, E., 2004. Biomass estimations and carbon stock calculations in the oil palm plantations of African derived savannas using IKONOS data. Int. J. Remote Sens. 25, 5447–5472.
Thenkabail, P.S., Schull, M., Turral, H., 2005. Ganges and Indus river basin land use/land cover (LULC) and irrigated area mapping using continuous streams of MODIS data. Remote Sens. Environ. 95, 317–341.
Thenkabail, P.S., Biradar, C.M., Noojipady, P., Cai, X., Dheeravath, V., Li, Y., Velpuri, M., Gumma, M., Pandey, S., 2007. Sub-pixel area calculation methods for estimating irrigated areas. Sensors 7, 2519–2538.

Thenkabail, P., GangadharaRao, P., Biggs, T., Gumma, M., Turral, H., 2007a. Spectral matching techniques to determine historical land-use/land-cover (LULC) and irrigated areas using time-series 0.1-degree AVHRR pathfinder datasets. Photogramm. Eng. Remote Sens. 73, 1029–1040.

Thenkabail, P.S., GangadharaRao, P., Biggs, T., Gumma, M.K., Turral, H., 2007b. Spectral matching techniques to determine historical land use/land cover (LULC) and irrigated areas using time-series AVHRR pathfinder datasets in the Krishna River Basin, India. Photogramm. Eng. Remote. Sens. 73, 1029–1040.

Thenkabail, P., Biradar, C., Noojipady, P., Dheeravath, V., Li, Y., Velpuri, M., Gumma, M., Reddy, G., Turral, H., Cai, X., Vithanage, J., Schull, M., Dutta, R., 2009a. Global irrigated area map (GIAM) for the end of the last millennium derived from remote sensing. Int. J. Remote Sens. 30 (14), 3679–3733.

Thenkabail, P.S., Biradar, C.M., Noojipady, P., Dheeravath, V., Li, Y., Velpuri, M., Gumma, M., Gangalakunta, O.R.P., Turral, H., Cai, X., Vithanage, J., Schull, M.A., Dutta, R., 2009b. Global irrigated area map (GIAM), derived from remote sensing, for the end of the last millennium. Int. J. Remote Sens. 30, 3679–3733.

Thenkabail, P.S., Knox, J.W., Ozdogan, M., Gumma, M.K., Congalton, R.G., Wu, Z., Milesi, C., Finkral, A., Marshall, M., Mariotto, I., 2012. Assessing future risks to agricultural productivity, water resources and food security: how can remote sensing help? Photogramm. Eng. Remote. Sens. 78, 773–782.

Thiruvengadachari, S., Sakthivadivel, R., 1997. Satellite Remote Sensing for Assessment of Irrigation System Performance: A Case Study in India. Research Report 9 International Irrigation Management Institute, Colombo, Sri Lanka.

Tilman, D., 1999. Global environmental impacts of agricultural expansion: the need for sustainable and efficient practices. Proc. Natl. Acad. Sci. 96, 5995–6000.

Tilman, D., Cassman, K.G., Matson, P.A., Naylor, R., Polasky, S., 2002. Agricultural sustainability and intensive production practices. Nature 418, 671–677.

Tomlinson, R., 2003. Thinking about Geographic Information Systems Planning for Managers. ESRI Press, p. 283.

Wan, Z., Wang, P., Li, X., 2004. Using MODIS land surface temperature and normalized difference vegetation index products for monitoring drought in the southern Great Plains, USA. Int. J. Remote Sens. 25, 61–72.

Wang, J., Ling, Z., Wang, Y., Zeng, H., 2016. Improving spatial representation of soil moisture by integration of microwave observations and the temperature–vegetation–drought index derived from MODIS products. ISPRS J. Photogramm. Remote Sens. 113, 144–154.

WMO, 2015. WMO (World Meteorological Organization) Press Release, 25-01-16. (Accessed 21 Aug 2015).

Yaduvanshi, A., Srivastava, P.K., Pandey, A.C., 2015. Integrating TRMM and MODIS satellite with socio-economic vulnerability for monitoring drought risk over a tropical region of India. Phys. Chem. Earth Parts A/B/C 83–84, 14–27.